Strongly gliding harmonic tremor during the 2009 eruption of Redoubt Volcano

Alicia J. Hotovec [a,*], Stephanie G. Prejean [b], John E. Vidale [a], Joan Gomberg [c]

[a] University of Washington, Department of Earth and Space Sciences, Box 351310, Seattle, WA 98195, USA
[b] United States Geological Survey, Volcano Science Center, 4210 University Dr., Anchorage, AK 99508, USA
[c] United States Geological Survey, University of Washington, Department of Earth and Space Sciences, Box 351310, Seattle, WA 98195, USA

ARTICLE INFO

ABSTRACT

During the 2009 eruption of Redoubt Volcano, Alaska, gliding harmonic tremor occurred prominently before six nearly consecutive explosions during the second half of the eruptive sequence. The fundamental frequency repeatedly glided upward from <1 Hz to as high as 30 Hz in less than 10 min, followed by a relative seismic quiescence of 10 to 60 s immediately prior to explosion. High frequency (5 to 20 Hz) gliding returned during the extrusive phase, and lasted for 20 min to 3 h at a time. Although harmonic tremor is not uncommon at volcanoes, tremor at such high frequencies is a rare observation. These frequencies approach or exceed the plausible upper limits of many models that have been suggested for volcanic tremor. We also analyzed the behavior of a swarm of repeating earthquakes that immediately preceded the first instance of pre-explosion gliding harmonic tremor. We find that these earthquakes share several traits with upward gliding harmonic tremor, and favor the explanation that the gliding harmonic tremor at Redoubt Volcano is created by the superposition of increasingly frequent and regular, repeating stick–slip earthquakes through the Dirac comb effect.

© 2012 Elsevier B.V. All rights reserved.

1. Introduction

Harmonic tremor is a continuous seismic and sometimes acoustic signal that often accompanies unrest on volcanoes of varying compositions and behaviors. Several narrow, evenly spaced peaks dominate the frequency spectrum of the signal: a fundamental tone and its overtones, with the fundamental tone usually in the range of 1 to 5 Hz (Neuberg, 2000; de Angelis and McNutt, 2007). Frequencies of the peaks often change with time, forming "gliding spectral lines" on spectrograms.

Behavior of harmonic tremor is highly variable from volcano to volcano, but can be roughly grouped by style of eruption. Harmonic tremor during times of high explosive activity can be complex, but upward gliding of harmonic tremor immediately prior to an explosion has been observed at Arenal Volcano, Costa Rica (Lesage et al., 2006), and Soufrière Hills Volcano, Montserrat (Powell and Neuberg, 2003). In both cases, the fundamental tone rose nearly monotonically from 1 to 3 Hz in the span of a few minutes. Chugging is a subset of harmonic tremor immediately following steam or Strombolian explosions, and is often accompanied by audible sounds and pulsed acoustic recordings. Chugging has been observed following Strombolian explosions at Mt. Semeru Volcano, Indonesia (Schlindwein et al., 1995), Arenal Volcano, Costa Rica (Benoit and McNutt, 1997; Hagerty et al., 2000; Lesage et al., 2006), Karymsky Volcano, Russia (Ozerov et al., 2003; Lees et al., 2004), Reventador Volcano (Johnson and Lees, 2000), Sangay Volcano (Lees and Ruiz,

2008), and Tungurahua Volcano (Ruiz et al., 2006), Ecuador, and following Vulcanian explosions at Sakurajima Volcano, Japan (Maryanto et al., 2008). The fundamental tone shifts both up and down in the range of 0.5 and 4 Hz, and lasts on the order of seconds to minutes. Alternatively, harmonic tremor can last minutes to hours during times of low explosive or eruptive activity. The fundamental tone remained steadily around 1 Hz for 18 h at Lascar Volcano, Chile (Hellweg, 2000), for at least 6 h at Veniaminof Volcano, Alaska (de Angelis and McNutt, 2007), and for almost 2 h at Erebus Volcano, Antarctica (Rowe et al., 2000). Reventador Volcano produced multiple cases of harmonic tremor with a fundamental tone of 2 Hz that glided slightly, and lasted tens of minutes to hours at a time (Lees et al., 2008). Periods of gliding from 5 to 9 Hz, and perhaps as high as 20 Hz, lasted for almost an hour at Stromboli Volcano, Italy, during a non-explosive phase of eruption (Ripepe et al., 2009).

Although gliding harmonic tremor is relatively common on active volcanoes, the mechanism producing the signal is still debated. A wide variety of models have been proposed that are capable of producing harmonics. The first model invokes the resonance of a fluid-filled crack, described by Chouet (1985). In this model, a hydrothermal crack, or the volcanic conduit itself, acts like a tube bell or flute, and harmonic overtones are produced by the multiple standing waves in the tube. Other models involve the resonance of gas-filled bubbles (Maryanto et al., 2008), or the vibration of the volcanic conduit inside an annulus (Jellinek and Bercovici, 2011). Another set of models utilizes the Dirac comb effect, in which the Fourier transform of a comb of evenly spaced, discrete pulses in time will produce evenly spaced harmonics in the frequency domain (mathematical details in the Appendix A). Often, non-linear fluid flow (Hellweg, 2000) or non-linear responses

* Corresponding author at: University of Washington, Department of Earth and Space Sciences, Box 351510, Seattle, WA 98195, USA. Tel.: +1 206 619 3958.
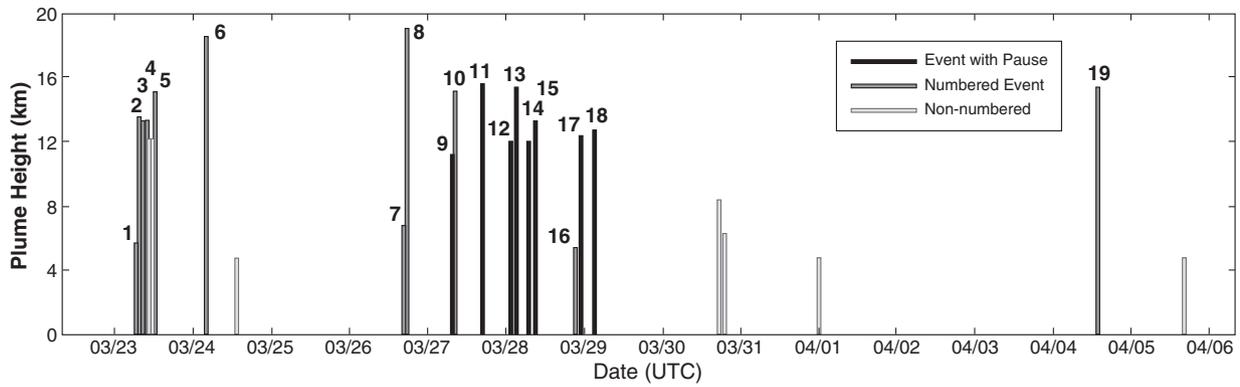E-mail address: ahotovec@uw.edu (A.J. Hotovec).

Fig. 1. Timeline of explosive events during the 2009 eruption. Height of plume is from FAA Nexrad radar and/or USGS radar at Kenai (Ekstrand et al., 2013). Events without numbers were identified upon reanalysis. Events preceded by a short silence are highlighted and discussed in later sections. After Schaefer (2012).

to fluid flow (Julian, 1994) are invoked as the source of these highly regular pulses. Each model has useful specific implications about conditions within the volcano, which are often difficult to constrain. A primary goal of this study is to identify the most plausible models that explain the observations of harmonic tremor from the 2009 eruption of Redoubt Volcano.

2. Gliding harmonic tremor

2.1. Summary of observations on Redoubt Volcano

Redoubt Volcano explosively erupted in March 2009 after 20 years of quiescence. Intermittent seismic activity began in January 2009, and some reports of degassing date back to July 2008 (Schaefer, 2012). This behavior is in stark contrast to the mere 23 h of pre-eruptive seismicity that heralded the 1989 eruption (Power et al., 1994; Power et al., 2013). The eruptive sequence began March 23, 2009, with a series of five major Vulcanian explosions spaced just over an hour apart. A second pulse of closely spaced explosions

followed between March 26 and March 29, 2009, most of which were preceded by upward gliding harmonic tremor. The entire sequence lasted two weeks, consisted of more than eighteen Vulcanian explosions with plume heights ranging from 4 to 18.8 km, and culminated in a major dome collapse on April 4, 2009 (Bull and Buurman, 2013). Fig. 1 shows a timeline of the explosive events, their associated plume heights, and the numbering scheme used to reference specific explosions of interest throughout this paper. A dome-building phase followed the last explosion, and began with unusually high extrusion rates (Bull et al., 2013; Diefenbach et al., 2013). This phase lasted until July 2009, and was also accompanied by periods of harmonic tremor and drumbeat earthquakes (Buurman et al., 2013).

2.1.1. Seismic instrumentation

The Alaska Volcano Observatory (AVO) operates a permanent seismic network near Redoubt Volcano of one L22 and seven L4 short-period seismometers (Fig. 2) (Dixon et al., 2010). Of these stations, REF and RED are 3-component, and remaining stations have
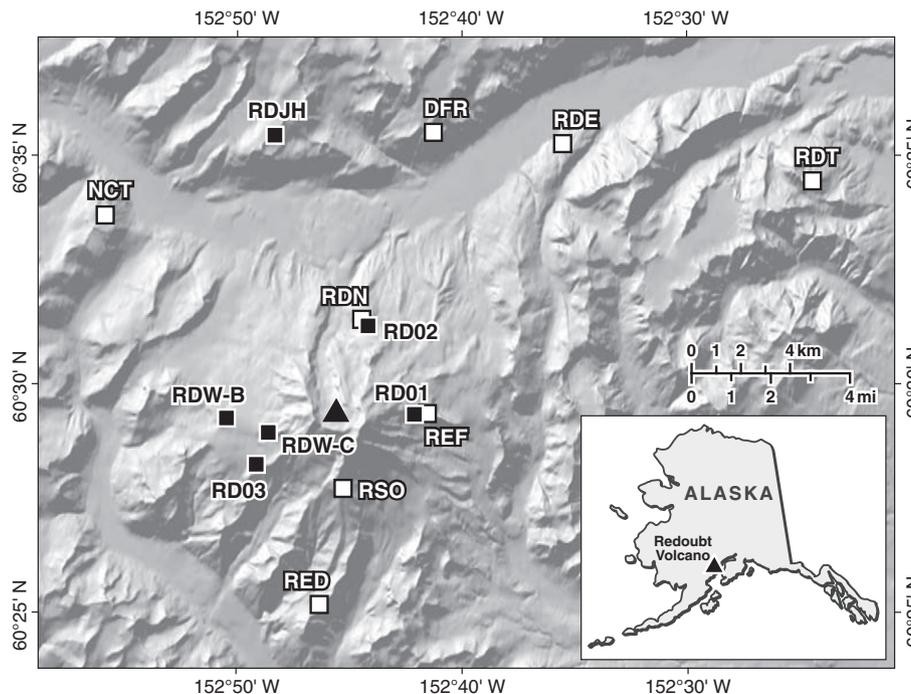

Fig. 2. Seismic network map. The black triangle marks approximate location of the active vent and dome. White squares are permanent short-period stations, and black squares are broadband stations.

only a vertical channel. The existing network was supplemented by six Guralp CMG-6TD 3-component broadband seismometers. RDJH was installed on February 4, 2009, and RDW-B on February 24, 2009; both were telemetered. Additional campaign stations (RD01, RD02, RD03, and RDW-C) were deployed on March 21, 2009, during the pre-eruptive sequence. Actual station coverage during the entirety of the eruptive sequence is poorer than the station map in Fig. 2 implies. Both RSO and RDJH went offline on March 25, 2009, and RED was often saturated with noise. DFR is co-located with an acoustic microphone that recorded infrasound of the explosive events.

2.1.2. Seismic signal characteristics

The focus of our study is gliding harmonic tremor present immediately prior to six nearly consecutive explosions on March 27 and 28 (Fig. 3), spanning Events 9 through 15. Many explosive events in the latter half of the eruptive sequence had a marked increase in seismicity in the minutes to hours before explosion, either as tremor or earthquake swarms (Buurman et al., 2013) followed by a seismic quiescence, but only six show gliding clearly. Table 1 summarizes these observations for Events 9 through 18.

Gliding tremor was recorded across the local network, and as far away as 90 km at both Spurr and Iliamna volcanoes for Events 9 and 13. Frequencies above 15 Hz were not recorded at more distant stations due to attenuation, but tremor frequencies approaching 20 to 25 Hz were apparent on multiple stations near the summit, and as

high as nearly 30 Hz at short-period station REF. Despite these high frequencies, the same evolution of harmonic tremor is seen on both campaign and telemetered stations, so we can rule out station noise and path effects as causes. Integer harmonic overtones exist for most events, but are usually weaker than the fundamental tone, and many events have only one overtone visible even at the closest stations. Harmonic tremor was never recorded infrasonically at DFR, but the associated explosions had energetic acoustic signals (Fee et al., 2013).

Pre-explosive gliding occurs on consecutive explosions between Events 9 and 15, with the possible exception of Events 10 and 11. Event 10 occurred just a few minutes after Event 9, so any gliding preceding this explosion might be buried in the previous explosion signal. Gliding prior to Event 11 is difficult to detect due to strong nonharmonic tremor that dominates the signal. Weak, upward gliding energy from 10 to 25 Hz exists across most of the network and up to 30 Hz at REF in the last 2 min before this explosion, followed by 30 seconds of relative quiescence. Because this behavior is generally consistent with the other events, we consider Event 11 to be part of the sequence.

The spectral evolution of gliding on Redoubt Volcano is reminiscent of, but at significantly higher frequencies than, pre-explosive gliding from 1 to 3 Hz on Soufriére Hills Volcano, Montserrat in 1999 (Powell and Neuberg, 2003). Over the six explosions, the fundamental tone spans the range of less than 1 Hz to upwards of 30 Hz,
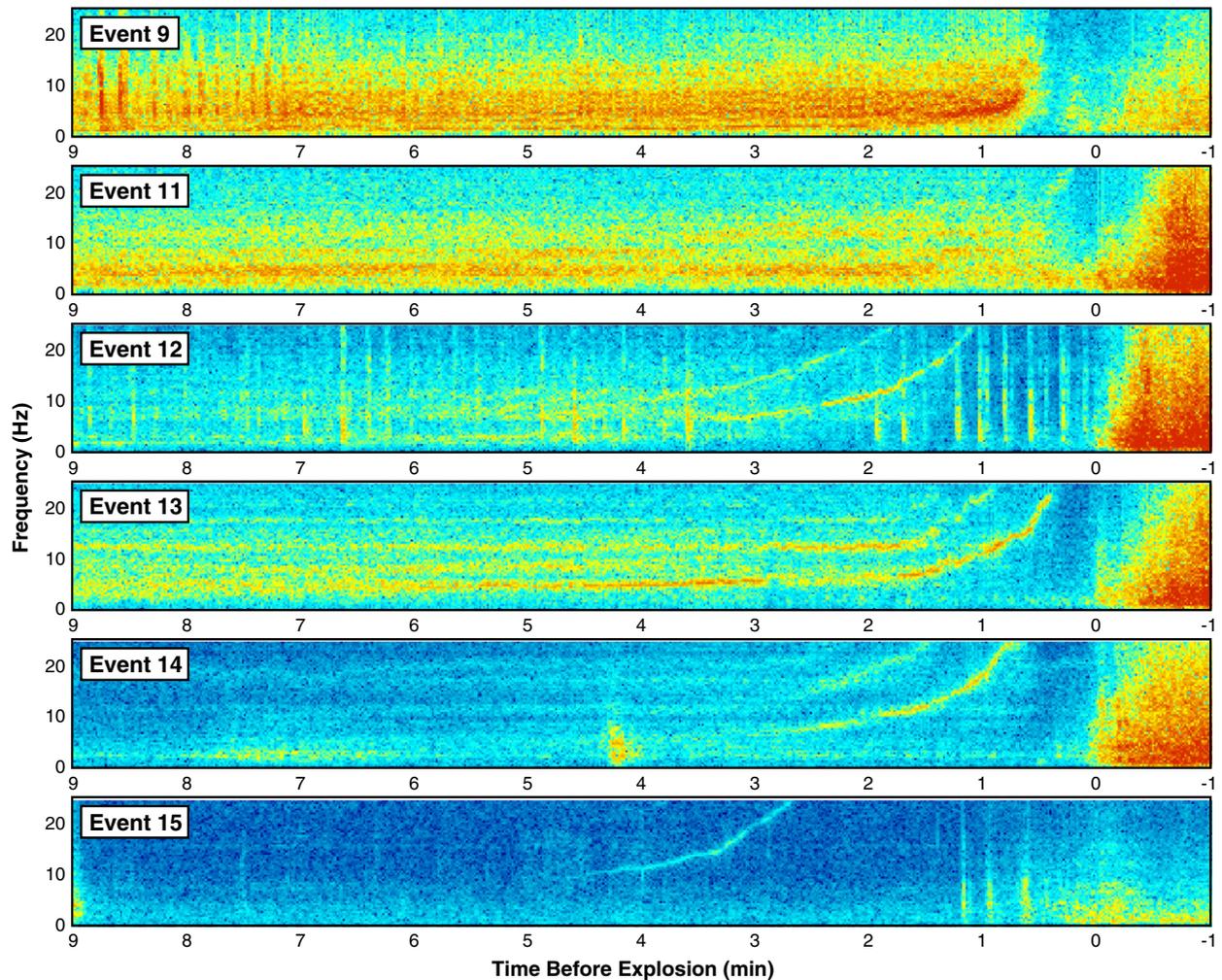

Fig. 3. Velocity spectrograms of the pre-explosive gliding harmonic tremor on station RD01, to the east of the vent. All spectrograms are plotted on a common logarithmic color scale using a 2-second 50% overlapping window. Times are aligned to the approximate explosion onset at $t = 0$, and frequency is plotted up to the broadband Nyquist frequency of 25 Hz. Bright vertical lines are earthquakes.

Table 1
Summary of gliding events. Plume heights from Bull et al. (2013). Lowest frequency with harmonics visible using a 10-second, 50% overlapping FFT window on any station. Highest frequency observed on station REF. Quiescence measured from time of highest observed frequency to explosion onset on REF, and rounded to the nearest 5 s. Repeating earthquakes are considered present if they can be correlated via waveform cross-correlation. Furthest distance is measured from furthest station where tremor is visible to dome. For Event 18, this applies to visibility of repeating earthquakes rather than harmonic tremor.

Event #	Time (UTC)	Plume height (km asl)	Explosion acoustic onset	Lowest harmonic frequency (Hz)	Highest harmonic frequency (Hz)	Approx. pre-explosive quiescence (s)	Repeating earthquakes detected	Furthest distance recorded (km)
9	03/27 07:47	12.5	Emergent	0.8	10	30	Yes	86
11	03/27 06:39	15.6	Impulsive	?	30	15	Yes	22
12	03/28 01:34	14.6	Impulsive	0.5	28	70	Yes	22
13	03/28 03:24	15.2	Impulsive	2	23	30	Maybe	86
14	03/28 07:19	14.6	Impulsive	7	30	45	No	4
15	03/28 09:19	14.6	Impulsive	10	25	180	No	3
17	03/28 03:29	12.5	Impulsive	0.5	?	240	Maybe	22
18	03/29 03:23	14.6	Emergent	n/a	n/a	180	Yes	12

and changes by as much as 20 Hz in 1 min. Both frequency range and rate of frequency change are similar for Events 12 through 15. Fig. 4 illustrates the high degree of repeatability in time evolution of the fundamental spectral line for these events, as well as its similarity to the simple rational function $f = 1/T$, where T is period, which is a linearly decreasing function of time. We also notice that harmonic tremor seems to start, or at least become visible, at higher frequencies for each new explosion. Due to low amplitudes at the highest frequencies, it is difficult to constrain how the highest frequency is changing from event to event.

After the tremor rises in frequency then fades, there is a quiet interval in the range of 15 to 270 s before an explosion. There is no consistent correlation between duration of the quiet time and either order of explosion, plume height, maximum frequency, or tremor amplitude. It is possible that the frequency of the tremor continues to climb unobserved, but because there is no evidence that is the case, we assume the interval is aseismic. Although they do not have the same dramatic gliding as earlier events, Events 17 and 18 also have similar quiet intervals prior to explosion. Harmonic tremor with fundamental frequency on the order of 0.5 Hz abruptly begins approximately 40 min prior to Event 17, but it eventually degrades into nonharmonic tremor that abruptly decays in amplitude immediately before the explosion. Small, increasingly frequent earthquakes that also abruptly stop precede Event 18. There is no clear silence before Event 16, 19, or any other previous explosion.

Because gliding tremor shares so many behavioral features among explosive events, we suspect a common, non-destructive source. Fundamental frequencies observed as high as 30 Hz strongly constrain
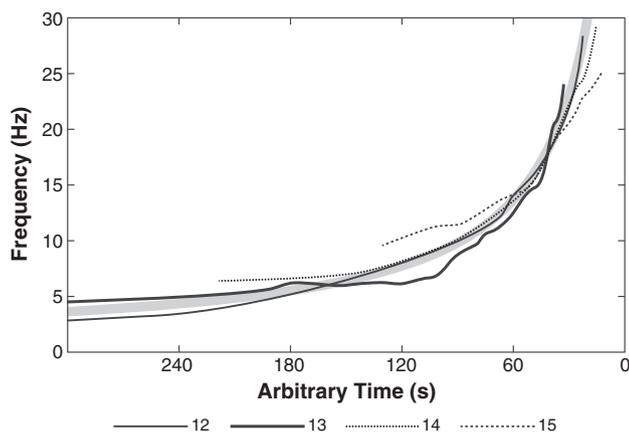
models to explain the tremor. Surprisingly, such high frequencies are not exclusive only to the explosive phase, as extended periods of high-frequency gliding were also observed beginning April 5, while the volcano was actively extruding a lava dome (Fig. 5). During this time, the fundamental tone remained over 15 Hz for nearly 20 min in multiple instances, compared to just a few seconds prior to the explosions. The fundamental tone oscillates wildly, gliding both up and down in frequency, although there seems to be a preference toward downward gliding. Tremor continues sporadically in two- to three-hour bursts until April 10, 17:30 UTC, and is accompanied by continuous swarms of earthquakes.

Although the temporal behavior of extrusive-phase gliding is different than that of pre-eruptive gliding, the unusually high frequency content suggests that the same or similar source may be at work for both time periods. Therefore, we require a model that can produce harmonics with a fundamental frequency up to 30 Hz, permits the dominant frequency to change monotonically in a matter of minutes, can stably remain at high frequencies for extended periods of time, can survive or be easily reestablished between multiple explosions, and is seismically powerful enough to have harmonics be recorded at distances of 20 to 100 km. If possible, the model should permit conditions expected in both the pre-explosive and extrusive phases of volcanic activity.

2.2. Evaluation of models

Many explanations for the source of harmonic peaks in volcanic tremor invoke resonance of a fluid-filled pipe or crack, such as the volcanic conduit (Chouet, 1985; Benoit and McNutt, 1997; de Angelis and McNutt, 2007; Maryanto et al., 2008). Gliding is attributed to changes in properties of a resonator, most often fluid acoustic velocity or effective resonator length (Neuberg, 2000; Jousset et al.,
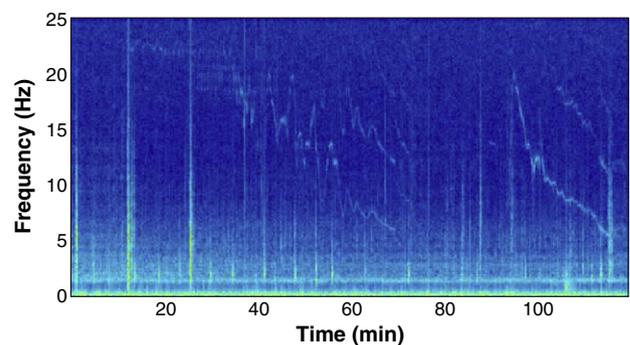

Fig. 4. Fundamental frequencies of four consecutive gliding events plotted on an arbitrary time axis, so that they align at $f = 18$ Hz. The lines are traced from a spectrogram of short period station REF, which has a Nyquist frequency of 50 Hz. The lines have repeatable shapes, though there is some variation in slope. Thick shaded line is a simple rational function, $f = 1/(-0.001\,t)$, where f is frequency (Hz) and t is time (s).

Fig. 5. Two-hour representative sample of harmonic tremor on station RDW-C during the extrusive phase, beginning April 5, 2009 08:00 UTC. Spectrogram was made using a 10-second 50% overlapping sliding window, and is plotted on the same color scale as in Fig. 3. Harmonic tremor with fundamental tones consistently above 5 Hz continued sporadically until April 10. This tremor was observed on several other stations in the network, both telemetered and untelemetered, but at lower amplitude.

2003). Although it is easy to visualize the rise and fall of a bubbly magma within the conduit as similar to a slide whistle, the excitation mechanism for the resonance itself is usually left unspecified.

Following these models we can calculate reasonable dimensions of the crack for a given frequency using the general equation for resonance of a tube with matched end conditions (open-open or closed-closed): $f = v/(2\,L)$, where f is frequency, v is acoustic velocity, and L is the length of the tube. The equation implies that if acoustic velocity alone changes, it must increase to 30 times its initial value for the case of Redoubt Volcano's tremor. This range is roughly equivalent to the difference in P-wave velocity between air and the upper mantle, but could be feasible for acoustic velocities well below 1 km/s if two-phase flow is involved. Alternatively, if we assume that acoustic velocity remains constant at that of bubbly water or gas-rich magma (roughly 1 km/s, after modeling by Jousset et al., 2003), a crack of 250 m length would produce 2 Hz harmonic tremor, and a crack of 16 m length would produce 30 Hz harmonic tremor. For Events 12 through 15, the crack must be consistently shortening at a rate of approximately 0.5 m/s, and perhaps closer to 2 m/s to reproduce the gliding at the end of Event 9. These lengths are for the matched end condition case; the lengths would be half as much for unmatched (open-closed) end conditions and produce only odd harmonics, which we do not observe. If we consider the resonating body to be the volcanic conduit, an acoustically impermeable layer, such as a bubble nucleation level, could be rising quickly and shortening the resonating portion of the conduit. Conversely, the resonating body could also be a thin hydrothermal crack that is collapsing on one or both ends, perhaps from increased pressure, and is then propped open again after each explosion (B. Chouet, personal communication, 2010). Although we only present the end members, it is possible that a linear combination of change in acoustic velocity and length occurred simultaneously.

The magma wagging model of Jellinek and Bercovici (2011) also describes conduit processes, but the frequency of tremor depends primarily on the width and properties of the annulus surrounding the conduit. However, for realistic combinations of conduit geometry, the range for which magma wagging is viable is 0.1 to 5 Hz, which is well below the range of observed frequencies at Redoubt Volcano. The model also requires the conduit to bend or other nonlinear effects to produce harmonic overtones (D. Bercovici and M. Jellinek, personal communication, 2011).

An alternative suite of models focuses on the flow of fluids through cracks. Julian (1994) proposes that harmonic tremor is a non-linear response to fluids flowing through constricted pathways, and that damping of the system will produce periodic oscillations. Alternatively, the harmonic nature of the signal could arise from constricted flow of the fluid itself, not unlike the whistle of a teakettle, with eddy shedding of steam being the most reasonable mechanism for our range of observed frequencies (Hellweg, 2000). Choked flow of gas near the surface can be consistent with the seismic and acoustic observations of chugging (Johnson and Lees, 2000). The choked flow mechanism might also be supplemented with feedback control through conduit resonance (Lesage et al., 2006). These models have mostly been applied to chugging, or to extended periods of tremor around 1 Hz in frequency. All these theories imply that higher flow rates are required for higher frequencies, and are heavily dependent on assumptions about flow dimension and Reynolds number. For Redoubt Volcano, this implies that the extended periods of high frequency tremor represent extended periods of high velocity fluid flow. The lack of acoustic signal suggests the source may not be gas escaping at the surface, but does not exclude the possibility of flow deeper within the edifice. It may also be that flow is poorly acoustically coupled or that the signal to noise ratio for the single microphone is too high to detect the gas release.

While fluid flow and degassing are ways of generating highly regular pulses of seismic energy, they are not necessarily the only ways.

For example, iceberg harmonic tremor is generated by repetitive stick–slip events as icebergs rub against each other in collisions (MacAyeal et al., 2008) or against the sea floor in shoaling events (Martin et al., 2010). The individual energy pulses are small, stick–slip icequakes, and the velocity of the drifting iceberg modulates the inter-event rate. Previous studies involving spectral character have indicated that low-frequency earthquakes and volcanic tremor may share a common source (Fehler, 1983). The sources of low-frequency and hybrid earthquakes are often also closely linked to the influence of fluids (Chouet, 1988; Matoza et al., 2009). Modeling has also indicated that at least some of the low-frequency content and spurious source mechanisms may be partly due to near-surface path effects (Malone and Haulter, 2003; Bean et al., 2008), and others have suggested brittle-failure as a mechanism (Iverson et al., 2006; Neuberg et al., 2006; Harrington and Brodsky, 2007). Regardless of source, multiple observations exist of swarms of low-frequency earthquakes merging into tremor on Soufriére Hills Volcano, Montserrat (Neuberg et al., 1998; Neuberg, 2000), and Miyakejima Volcano, Japan (Fujita et al., 2009), and both in and out of tremor on Mount St. Helens, Washington (Malone and Qamar, 1984), and Augustine Volcano, Alaska (Power and Lalla, 2010). The highly repetitive and periodic nature of some earthquake swarms, such as "drumbeat" swarms on Mount St. Helens (Moran et al., 2009), seem to mimic the periodic nature of harmonic tremor but at much slower rates.

3. Closely repeating earthquakes and harmonic tremor

A large swarm of repeating earthquakes preceded the first onset of harmonic tremor before Event 9 (Buurman et al., 2013). While this observation alone is not extraordinary, we find that earthquakes comprising the swarm prior to Event 9 occur increasingly frequently as the time approaches the explosion, until they blend into harmonic tremor. Event 11 also had a small swarm prior to nonharmonic tremor, and Event 12 had a swarm prior to and concurrently with harmonic tremor. The simplest hypothesis proposes that the earthquakes and tremor are related, and possibly even resulting from the same physical process.

The first test of our hypothesis is that the earthquakes all must originate from a single source. If the earthquakes were widely distributed in space, at each station the waveforms and arrival times would differ from earthquake to earthquake, and may be too irregular to form harmonics. However, if the earthquakes share the same location, timing will only depend on when the earthquakes actually occurred, and their waveforms will be highly similar if we assume they also share the same source mechanism. We measure waveform similarity using waveform cross-correlation, following previous studies that employed cross-correlation and multiplet analysis on volcanic earthquake swarms, especially those of low-frequency nature (e.g., Stephens and Chouet, 2001; Caplan-Auerbach and Petersen, 2005; Green and Neuberg, 2006; Umakoshi et al., 2008; Buurman and West, 2010; Thelen et al., 2010).

Of the earthquakes in the swarm preceding Event 9, 267 were large enough to be located with the permanent local network by AVO (Dixon et al., 2010). We high pass filtered the seismograms from those earthquakes above 0.5 Hz to reduce microseism noise on the broadband stations, and then cross-correlated over a 15-second, amplitude-normalized window starting on the P-wave arrival. Approximately 95% of these seismogram pairs have normalized correlation coefficients greater than 0.85, and at least 75% correlate with coefficients in excess of 0.95. In fact, those earthquakes that do not correlate as highly generally contain more than one earthquake within this time window. Closer analysis of broadband data revealed many additional earthquakes with visually similar waveforms that were missing from the AVO catalog. To make the catalog with repeating earthquakes from this family more complete, we

used the largest earthquake on the vertical component of broadband station RDW-C as a template to find other similar earthquakes. We scanned the continuous data over a 3-second sliding window, and set the threshold for a potential match at a generous correlation coefficient of 0.5. This is a variation of a method used to find repeating long-period earthquakes prior to the 1989 eruption of Redoubt Volcano (Stephens and Chouet, 2001), and was also utilized for repeating coupled earthquakes at Shishaldin Volcano, Alaska (Caplan-Auerbach and Petersen, 2005), and repeating explosions of Pavlof Volcano, Alaska (Haney et al., 2009).

We found 1691 additional matches with correlation coefficients greater than 0.5, with 483 of these having coefficients greater than 0.75 during this swarm. The largest earthquakes correlate best with few exceptions. That is, as amplitude decreases, so too does the signal-to-noise ratio and correlation coefficient (Fig. 6). We note that there is a bimodal amplitude distribution, with alternating large and small earthquakes that appear to be part of the same family. The detector only seemed to miss the smallest earthquakes for which only a small S-wave was visible, or when earthquake waveforms began to significantly overlap in the last hour leading up to the gliding. Between 5 and 50 additional matches, depending on coefficient cutoff and window size, were found within the harmonic tremor where the amplitude of individual events was large enough to overpower the harmonics. It is also worth noting that the amplitudes of the small earthquakes increase smoothly with time until they are consistent with the amplitude of the harmonic tremor. This detector was also applied to the earthquakes prior to Event 12, but we found a much more complicated time series with lower amplitudes and cross-correlation coefficients. Therefore, we focus on Event 9 because it has the clearest matches, and is the most temporally regular swarm.

A second test of our hypothesis is that the changing periodicity of the earthquakes should be compatible with the frequencies at which we observe tremor. That is, the inverse of the smallest inter-event period measurable from between earthquakes should be just slightly lower than the lowest fundamental frequency of the harmonic tremor. We measured the P-wave arrival time for each earthquake at station RD01 through waveform cross-correlation of matched earthquakes down to a correlation coefficient of 0.5 over a 3-second window. RD01 was chosen for its clear, impulsive arrivals for both large and small earthquakes. First arrival times were supplemented in the
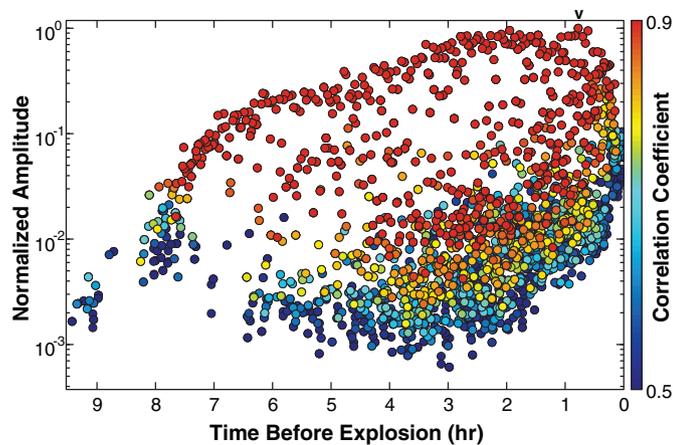
last 2 h by hand picks where we had reason to believe that the detector skipped an earthquake. Most of these missed earthquakes were buried in the surface waves of larger events or were small; they were objectively identified by simultaneously looking at a spectrogram, a high-pass filtered trace at 0.5 Hz, and a second high-pass filtered trace at 10 Hz. Where visible, the first P-wave motion was hand picked. In many cases, the P-wave was not clearly visible, but the S-wave arrival was. For these cases, we assumed the P-wave arrived 1 second before the S-wave. Hand picking became difficult around 20 min prior to explosion, where the time between earthquakes approached the time between the arrival of the P- and S-waves.

Fig. 7 shows quantitatively how the timing between individual earthquakes decreases as a function of time. Although the timing errors in hand picked arrivals and skipped earthquakes increases with time in the sequence, the earthquakes seem to become more regularly spaced with time. The percent error in periodicity, defined as the standard deviation of the periodicity divided by the mean periodicity for a bin of 100 earthquakes, reaches a minimum at 25%, but likely overestimates the actual variation. Regardless of these errors, our measurements should still provide useful first-order estimates of the change in period with time. We sampled the fundamental frequency of the harmonic tremor during Event 9 from a spectrogram on the same station, and then plotted its inverse, or period, on the same axes as the earthquakes. The average inter-earthquake time approaches the period of the tremor. Remarkably, a least squares linear trend of the inter-earthquake period has a slope of roughly −0.001 s/s, which is the same slope used to fit the period of gliding tremor from Events 12 through 15 in Fig. 4.

We further tested our hypothesis that the tremor is comprised of regularly repeating earthquake signals through a series of synthetic experiments. We verified that earthquakes that repeat with sufficient regularity could produce harmonics through the Dirac comb effect, in which frequency of the fundamental tone is inversely related to the timing between sources (Powell and Neuberg, 2003). We summarize the mathematical underpinnings of this effect in the Appendix A. Powell and Neuberg (2003) state in a similar analysis that in order to produce harmonics through the comb effect, the error in periodicity of the sources must be less than 2% to reproduce features of the tremor observed on Lascar, and Hagerty et al. (2000) attest that the error must be less than 1% to reproduce the tremor on Arenal. Harmonic tremor at Redoubt had fewer overtones than Lascar and Arenal, so we reconsider the allowable variability in timing and amplitudes of repeating earthquakes necessary to be consistent with the tremor we observe.
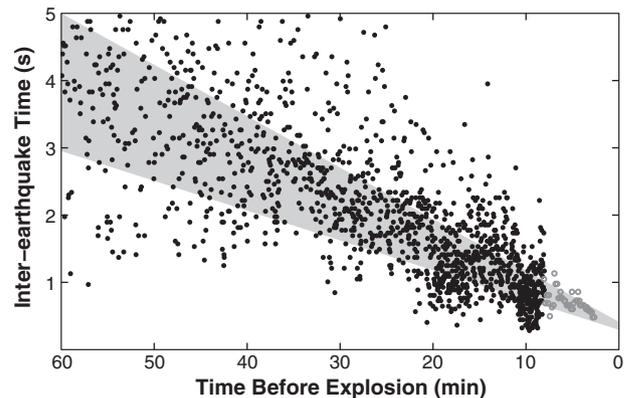

Fig. 6. Normalized amplitude and correlation coefficient with respect to largest earthquake from before Event 9, marked with a 'v'. Amplitude is based on the maximum velocity amplitude of the S-wave, and is then normalized to the amplitude of the largest earthquake. Correlation coefficient is computed over a 3-second window beginning on the P-wave arrival. Longer window times do not significantly decrease the coefficient except where earthquakes begin to overlap. Color scale has been cropped between 0.9 and 0.5 to highlight the smooth gradient between correlation coefficient and amplitude. The relative amplitude of the subsequent harmonic tremor ranges from approximately 5×10^{-2} to 1×10^{-1}.

Fig. 7. Change in period between earthquakes (black dots) and period of tremor (open gray circles) over the last hour leading up to Event 9, with least squares linear trend line fit to the full ten-hour swarm of slope −0.001 s/s and thickness 25% of period (bold gray line). Period of tremor was measured by taking the inverse of the frequency of the fundamental tone from Fig. 3.

We constructed synthetic harmonic tremor by convolving an earthquake from a swarm prior to Event 9 with a pulse train of linearly decreasing recurrence interval with time, from 0.4 to 0.02 s over 6 min (Fig. 8). Variability in timing was included by adding Gaussian noise centered on the period between each earthquake, such that the percentage variation of interval remains constant despite changing frequency. We find for harmonic tremor with few overtones, as we see on Redoubt Volcano, that the period may vary by as much as 10% without destroying the first overtone, and by nearly 20% without destroying the fundamental tone. It is also important to note, especially for lower frequencies, that the choice of FFT window length affects the resolution of the harmonics. The spectrum becomes more peaked as more repeating pulses are included in the window, but becomes less harmonic if the time between these pulses changes sufficiently over the window.

We also evaluated the allowable variation in amplitude by adding Gaussian noise to the amplitude of the pulse train, and found that even 100% noise in amplitude does not significantly alter the harmonic nature of the signal. While we cannot separate individual earthquake signals during the interval in which we observe the harmonic tremor, the variability of the earthquake inter-event periods and amplitudes measured in the hours leading up to the tremor decreases with time such that just prior to the tremor it is of the order of the 20% and 100% limits, respectively, inferred in our synthetic tests. Moreover, even for spectrograms constructed with longer windows we do not observe harmonics prior to the last few minutes. In other words, the synthetic tests are consistent with the observations.
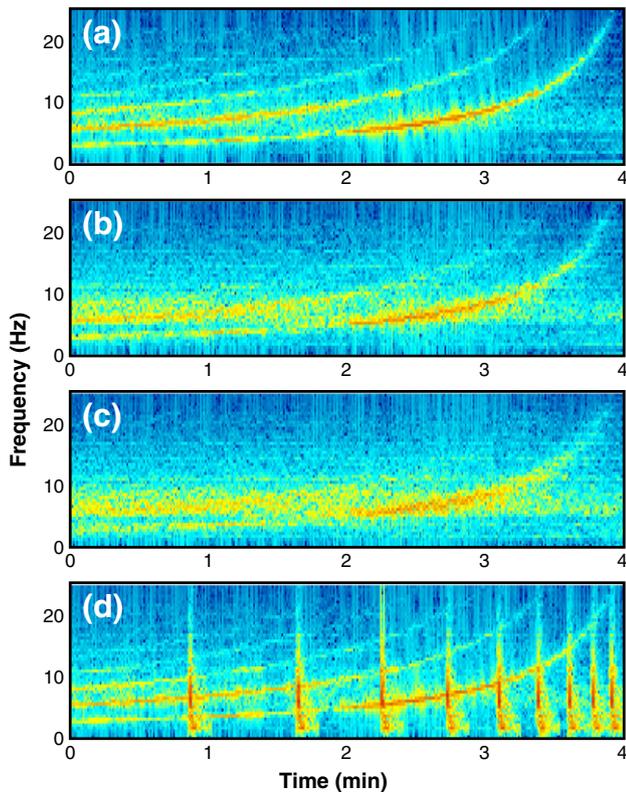
Physically they imply that in the hours leading up to the explosions the earthquakes occur both with increasing rate and regularity.

Our hypothesis that the tremor is comprised of repeating earthquakes also predicts that the two signals should also share the same spectral characteristics in the nonharmonic portion of the spectrum, since the total spectrum of tremor is the combination of the earthquake's spectrum and a comb (Garces and McNutt, 1997). Thus, our third test makes an effort to compare the tremor spectrum with a single repeating earthquake's spectrum. Fig. 9 shows the normalized spectrum of one of the repeating earthquakes with the average spectrum of 10 min of harmonic tremor immediately prior to Event 9. We averaged the tremor spectra over a time period when the harmonic peaks change dramatically to let the nonharmonic character dominate the spectrum, even though harmonics are present in shorter time windows. In this case the tremor spectrum should simply be the sum of multiple copies of the spectrum of a single earthquake, and the comb effect is reduced because the time between copies is insufficiently regular over the longer time period. Although the relative amplitudes of spectral peaks are slightly different, the earthquake and tremor spectra share highly similar shapes across the network.

Given that the earthquakes in the swarm prior to Event 9 appear to merge into harmonic tremor, and may indeed comprise it, we investigated the possible source mechanism of these earthquakes by further analyzing the spectra of the signals they generate. We note that the spectral content of these earthquakes is rich in frequencies above 5 Hz, and that many stations located on the volcano proper have waveforms with clearly impulsive arrivals. Based on classification of volcanic earthquakes by Lahr et al. (1994), these earthquakes most closely resemble shallow volcano-tectonic (VT) earthquakes. Often, VT earthquakes are attributed to brittle failure, and should theoretically have the same source spectra as non-volcanic earthquakes of the same size. Following Prejean and Ellsworth (2001), we computed fits of the P-wave spectra for large, similarly sized repeating earthquakes on multiple stations to both ω^2 and ω^3 source models (Brune, 1970) for a range of corner frequencies and seismic quality (Q) factor. Because uncorrected path effects may heavily contaminate spectra and because impulsive high-frequency earthquakes can have non-double couple moment tensors (e.g., Foulger et al., 2004), we use this analysis as a simple test to explore general consistency with the models, rather than to establish specific source parameters. Spectral fits were checked for consistency across the network. We find the best fitting source spectra for these M_d 1.0–1.7 earthquakes are consistent with an ω^2-source model with a corner frequency above 20 Hz and Q between 6 and 30 depending on seismic station used. Unfortunately, there is a heavy tradeoff between corner frequency
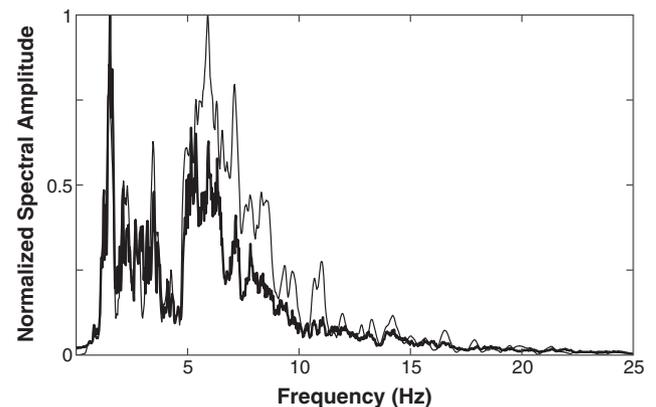

Fig. 8. Synthetic harmonic tremor was made by convolving a comb function of linearly decreasing period with time and a sample earthquake from the Event 9 swarm on station RDW-C. Error in periodicity of the comb with standard deviation of (a) 5%, (b) 10%, and (c) 15% degrades the harmonic nature of the signal. Random amplitude variation did not significantly alter the signal, but a few significantly larger outliers of the same family, as in (d), creates the appearance of simultaneous earthquakes and harmonic tremor. Purely horizontal bands across the spectrogram match the source earthquake's spectrum. The weak fundamental tone between 1 and 2 min coincides with a trough in the earthquake spectrum, giving the illusion of a missing fundamental tone.

Fig. 9. Normalized spectrum of a single repeating earthquake (thin line) vs. 10 min of tremor (thick line), both from prior to Event 9 on station RDW-C. Spectrum for the earthquake was calculated over a 30-second window, and the spectrum for tremor was averaged over 30-second long, 10-second overlapping sliding windows to enhance the nonharmonic part of the spectrum.

and Q, where lower Q will yield higher corner frequency. Q is not well constrained, though stations with consistently low-Q fits had broadband sensors installed temporarily on unconsolidated ash. Additionally, the Nyquist frequency for the broadband instruments is 25 Hz and the close short-period stations clipped on these earthquakes, so little reliable data are available to fully constrain the high corner frequencies one might expect for this magnitude range.

To further constrain the earthquake source properties, we stacked similar waveforms to resolve clear first motions on 12 stations, which included one station from both Spurr and Iliamna volcanoes, 90 km distant. First motions were mixed, with first compressional motion on stations to the north and east, and dilatational to the south and west (Fig. 10). These mixed first motions contrast observations of repeating long-period earthquakes with all dilatational first motions during the previous eruption of Redoubt Volcano in 1989–90 (Chouet et al., 1994), and the 2004 eruption of Mount St. Helens (Matoza et al., 2009). Fortuitously, many of the earthquakes in this swarm were large enough to be located, enabling us to solve for a focal mechanism. According to double difference relocations by Wessale et al. (2010), earthquakes in this swarm locate approximately 250 m WSW of the surface vent, roughly 300 m below sea level, and within 200 m of each other. We determined takeoff angles by assuming the average double-difference location and depth (Wessale et al., 2010), then traced rays through AVO's local 1-D velocity model for Redoubt Volcano (Dixon et al., 2010). We first solved for an initial double-couple fault plane solution with FPFIT (Reasenberg and Oppenheimer, 1985), and then further constrained the possible focal mechanism with P/S ratios for the closest stations using HASH v1.2 (Hardebeck and Shearer, 2002). Table 2 lists the motions and P/S ratios used in this inversion. The resulting fault plane solution is close to pure dip-slip (Fig. 10). However, although we can easily fit a double-couple mechanism to these earthquakes and the spectral fits are consistent with a double-couple mechanism, we do not have enough station coverage to perform a reliable full moment tensor inversion.

4. Discussion

We believe the best explanation for the observed gliding tremor at Redoubt Volcano is that it is composed of repeating earthquakes. We base this on observations of a smooth transition between the inter-event times of discrete earthquakes and frequency of harmonic

Table 2
List of first motions and P/S ratios used in the determination of focal mechanism.

Station	First motion	P/S ratio
DFR	Down	0.31
INE	Up	–
NCT	Down	1.70
RD01/REF	Down	0.28
RD02/RDN	Down	0.28
RD03	Up	0.14
RDE	Down	0.87
RDT	Down	0.44
RDW-B	Up	0.57
RDW-C	Up	0.23
RED	Up	0.53
SPU	Down	–

tremor prior to Event 9, the similarity in spectrum of the tremor window and an earthquake, and the fact that we can reproduce all the features of the observations with synthetic time series. Although Event 9 has the clearest supporting evidence, it is possible to explain the behavior of the following explosions in terms of this model. For Event 11, the majority of the pre-explosive tremor is nonharmonic, with only faint high frequency gliding visible near the end. A small swarm of earthquakes is visible prior to tremor, but with less regularity than Event 9. Our model is consistent with this event if earthquakes comprising the tremor were too irregularly spaced in time to form harmonics until the end. Event 12 had a large swarm of repeating earthquakes prior to and concurrent with gliding up to the onset of explosion that at times would blend in and out of harmonic tremor if long enough windows were used. Like Event 9, there seems to be a bimodal amplitude distribution based on waveform cross correlations, with small, more frequent earthquakes comprising tremor, and larger earthquakes of the same family individually visible. However, the behavior is much less regular in time than Event 9 for reasons we do not understand. Events 13 – 15 have few, if any, visibly repeating earthquakes. Thus consistency between our model and these events requires that the swarms become large enough to be detected when the inter-event rate is too high to see individual repeaters. The explosion associated with Event 16 had different acoustic character from the previous explosions (Fee et al., 2013), and we suppose that the source either did not have time to re-establish itself or was even destroyed in this event. Event 17 marks the return of
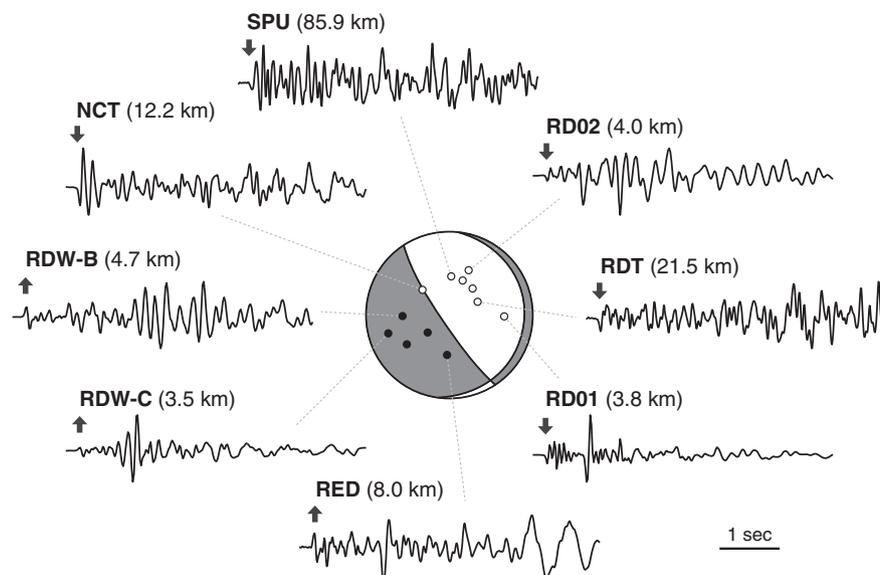

Fig. 10. Stack of repeating earthquakes prior to Event 9 at multiple stations showing difference in first motions and character of signal with both distance and azimuth. Traces are 5 s long, and normalized to the same maximum amplitude. Respective first motions are plotted on the best fitting focal sphere constrained by both first motion and P/S ratio.

repeating earthquakes and low-frequency harmonic tremor, but the signal eventually degrades into nonharmonic tremor. We interpret that the nonharmonic tremor is still composed of repeating earthquakes with irregular periodicity, as was possibly the case for Event 11. Event 18 has some repeating earthquakes that become more frequent, but do not become frequent enough to form harmonic tremor over our chosen window length before explosion. Finally, although frequency of tremor during the extrusive phase is considerably more variable with time than that of pre-explosive tremor, differences in behavior may be related to changes in extrusion rate (Diefenbach et al., 2013), eruptive style, or magma properties (Coombs et al., 2013) and subsequently on processes controlling earthquake repeat rate.

Proximity of repeating earthquakes to the inferred location of the conduit and high-angle faulting make a case for slip at or near the edge of the conduit wall. Stick–slip phenomena in the conduit have been attributed to cyclic eruptive activity (Denlinger and Hoblitt, 1999) and chugging (Ozerov et al., 2003), but these are on longer time scales than we observe. We suppose that slip in our case could represent brittle failure of viscous magma at the conduit wall itself as the magma ascends, as has been proposed as a possible mechanism for hybrid and long period earthquakes (Iverson et al., 2006; Neuberg et al., 2006; Harrington and Brodsky, 2007). Conceptually, as magma rises in the conduit, it cools near the top and along the edges, and may fracture under high enough strain-rate. Tuffen et al. (2008) demonstrated this phenomenon for magma in the lab at 900 °C, and showed that this fracture mechanism produces similar seismic signals as tectonic earthquakes. If we believe that our repeating earthquakes are similar to tectonic earthquakes of comparable size, the stressing rates required to have even a few earthquakes per second still seem abnormally high. It is possible that unusual material properties in the conduit region violate traditional assumptions about earthquake source mechanics such as stress drop. It is also unclear at this point exactly what force is causing the rate of occurrence to increase and become more regular immediately prior to these explosions. Acoustic character (Fee et al., 2013) and ashfall analysis (Wallace et al., 2013) of this subset of explosions indicates that the magma that erupted was possibly more viscous than in earlier explosions. Although viscosity may play a strong role in this model, there are many other variables that could conceivably control the rate of earthquake repetition, but a thorough investigation of these poorly constrained degrees of freedom is beyond the scope of this paper. However, it is clear that the process is repeatable between explosions, and returns when magma is extruded at the surface during dome building.

We infer that part of the repeatability between explosions has to do with the depth of the earthquakes, and therefore the harmonic tremor. Although the earthquakes are located near the conduit, they are relatively deep (Wessale et al., 2010). When the volcano erupts in a Vulcanian explosion, the conduit drains down the top 0.5 to 2 km (Druitt et al., 2002). If we believe the earthquakes locate at 300 m below sea level, or roughly 3 km below the surface vent, the earthquake and tremor source would be well below the fragmentation front, and remain intact through the explosion. The process repeats again in similar fashion as the conduit refills, and conditions for failure are met.

A curious and significant detail we have not yet discussed is the nearly aseismic period between the highest frequency tremor and the onset of explosion. One could imagine that the frequency of the fundamental tone actually exceeds 30 Hz, and is attenuated away or too low in amplitude to be recorded. Although we could argue this may be the case for Event 12, where earthquakes occur even during the otherwise quiet pause, the earthquakes prior to Event 18 clearly cease 3 min before the explosion. Whether this cessation in seismicity is caused by a temporary transition from stick–slip to aseismic sliding, a pause in movement, or whether some other pre-explosive process is at work is still an open question.

Even though we have presented evidence to support the hypothesis that harmonic tremor is composed of repeating earthquakes, we are still left with several other important and unanswered questions regarding this model. For example, why are the repeat rates and tremor frequencies for Redoubt Volcano so much higher than other, similar volcanoes? For that matter, what stressing rate is required to produce upwards of 30 small earthquakes per second, and is that feasible to apply to both phases of eruption? Why is the decrease in the period between the earthquakes and the period of the harmonic tremor linear? Interestingly, the linearly decreasing period in harmonic tremor does not appear to be unique to Redoubt Volcano alone, as the upward gliding harmonic tremor from Soufriére Hills Volcano also has a nearly linear shape when plotted in terms of period. Soufriére Hills Volcano also exhibited a linear increase in number of earthquakes over several swarms prior to dome failure (Hammer and Neuberg, 2009), which was proposed to be in line with the material failure law (Voight, 1988). With more study, we hope similar observations of gliding tremor can be applicable to forecasting behavior of other volcanoes in the short term.

5. Conclusions

Redoubt Volcano produced repeatable, upward gliding harmonic tremor preceding six explosive events, for which the fundamental tone spanned from <1 Hz to 30 Hz. Harmonic tremor with fundamental frequencies consistently above 10 Hz returned for several hours during the early extrusive phase. This frequency range greatly exceeds other observations of harmonic tremor, and has implications for the applicability of previously proposed tremor sources that work in the 1 to 5 Hz range. We find that the most likely source of harmonic tremor for Redoubt Volcano is that of repeating earthquakes through the Dirac comb effect, based primarily on the observation of a smooth transition between the inter-event time of repeating earthquakes and fundamental period of harmonic tremor prior to Event 9. Further investigation into the source of these earthquakes points toward a shear source near the conduit, deep enough to survive a series of explosions. Although we do not have a complete explanation for why the earthquake rate speeds up and becomes more regular prior to explosion, we believe these observations can inform future studies of pre-explosive conduit dynamics.

Appendix A

A Dirac comb is an infinite series of evenly spaced Dirac delta functions in time, which has the special property that its Fourier transform is a comb function in frequency as well. The spacing of the delta functions in frequency is the inverse of the period between delta functions in time.

We can represent a comb function as a series of incrementally phase shifted delta functions:

$$g(t) = \delta(t) + \delta(t-\tau) + \delta(t-2\tau) + \cdots + \delta(t-N\tau) + \cdots \qquad (A.1)$$

whose Fourier transform can be represented as a geometric series:

$$G(\omega) = 1 + e^{-i\omega\tau} + e^{-i\omega 2\tau} + \cdots + e^{-i\omega N\tau} + \cdots \tag{A.2}$$

Strictly speaking, a true comb function contains an infinite number of phase shifted delta functions. In practice, we only have a limited number of copies within a finite time window. Let us consider the case where we have only $N+1$ pulses with period τ over the window $t=0$ to $t=N\tau$. We can simplify the first $N+1$ terms of a geometric series as:

$$G(r) = 1 + r + r^2 + r^3 + \cdots + r^N = \frac{1-r^{N+1}}{1-r} \tag{A.3}$$

where in our case:

$$r(\omega) = e^{-i\omega\tau} \tag{A.4}$$

By substituting Eq. (A.4) into Eq. (A.3), and using both Euler's formula ($e^{ix} = \cos x + i \sin x$) and the double angle formulae, we find that the spectrum of a sequence of $N+1$ equally spaced delta functions is:

$$G(\omega) = e^{-\frac{1}{2}i\omega\tau} \frac{\sin\left(\frac{1}{2}\omega(N+1)\tau\right)}{\sin\left(\frac{1}{2}\omega\tau\right)} \tag{A.5}$$

The ratio of the two sin functions is essentially a periodic sinc function, with maxima where $(1/2)\omega\tau = \pi$. This occurs at integer frequencies $f = n/\tau$, the same as the true Dirac comb. Unlike the Dirac comb, the peaks of $G(\omega)$ have finite width, which can be approximated as $\Delta f \cong 1/(N\tau)$, and finite maximum amplitude $N+1$. Clearly, the larger N is (more repeats) the narrower the peaks become and the more harmonic the spectrum appears.

In our model, the repeating function is not a delta function, but a repeating earthquake. Thus, the total spectrum is the product of $G(\omega)$ and the spectrum of an earthquake. The harmonic frequencies of the spectrum are governed completely by the repeat interval, τ, but provide information about the earthquake spectrum where $G(\omega)$ is nonzero. It should be noted that earthquake spectra have finite bandwidths, typically decreasing with increasing frequency above some 'corner frequency' f_c. Finally, the harmonic nature of the signal may not be discernable for low values of N, even for perfectly timed repetitions, given the finite width and lower amplitude of the 'comb'.

References

Bean, C., Lokmer, I., O'brien, G., 2008. Influence of near-surface volcanic structure on long-period seismic signals and on moment tensor inversions: simulated examples from Mount Etna. Journal of Geophysical Research 113, B08308.

Benoit, J.P., McNutt, S.R., 1997. New constraints on source processes of volcanic tremor at Arenal Volcano, Costa Rica, using broadband seismic data. Geophysical Research Letters 24, 449–452.

Brune, J.N., 1970. Tectonic stress and the spectra of seismic shear waves from earthquakes. Journal of Geophysical Research 75, 4997–5009.

Bull, K.F., Buurman, H., 2013. An overview of the 2009 eruption of Redoubt Volcano, Alaska. J. Volcanol. Geotherm. Res. 259, 2–15.

Bull, K.F., Anderson, S.W., Diefenbach, A.K., Wessels, R.L., Henton, S.M., 2013. Emplacement of the final lava dome of the 2009 eruption of Redoubt Volcano. Alaska. J. Volcanol. Geotherm. Res. 259, 334–348.

Buurman, H., West, M.E., 2010. Seismic Precursors to Volcanic Explosions During the 2006 Eruption of Augustine Volcano. In: Power, J.A., Coombs, M.L., Freymueller, J.T. (Eds.), The 2006 Eruption of Augustine Volcano, Alaska: U.S. Geological Survey Professional Paper 1769, pp. 41–57.

Buurman, H., West, M.E., Thompson, G., 2013. The seismicity of the 2009 Redoubt eruption. J. Volcanol. Geotherm. Res. 259, 16–30.

Caplan-Auerbach, J., Petersen, T., 2005. Repeating coupled earthquakes at Shishaldin Volcano, Alaska. Journal of Volcanology and Geothermal Research 145, 151–172.

Chouet, B., 1985. Excitation of a buried magmatic pipe: a seismic source model for volcanic tremor. Journal of Geophysical Research 90, 1881–1893.

Chouet, B., 1988. Resonance of a fluid-driven crack: radiation properties and implications for the source of long-period events and harmonic tremor. Journal of Geophysical Research 93, 4375–4400.

Chouet, B.A., Page, R.A., Stephens, C.D., Lahr, J.C., Power, J.A., 1994. Precursory swarms of long-period events at Redoubt Volcano (1989–1990), Alaska: their origin and use as a forecasting tool. Journal of Volcanology and Geothermal Research 62, 95–135.

Coombs, M.L., Sisson, T., Bleick, H.A., Henton, S., Nye, C., Payne, A., Cameron, C., Larsen, J., Wallace, K., Bull, K., 2013. Andesites of the 2009 eruption of Redoubt Volcano. Alaska. J. Volcanol. Geotherm. Res. 259, 349–372.

de Angelis, S., McNutt, S.R., 2007. Observations of volcanic tremor during the January–February 2005 eruption of Mt. Veniaminof, Alaska. Bulletin of Volcanology 69, 927–940.

Denlinger, R.P., Hoblitt, R.P., 1999. Cyclic eruptive behavior of silicic volcanoes. Geology 27, 459–462.

Diefenbach, A.K., Bull, K.F., Wessels, R.L., McGimsey, R.G., 2013. Photogrammetric monitoring of lava dome growth during the 2009 eruption of Redoubt Volcano. J. Volcanol. Geotherm. Res. 259, 308–316.

Dixon, J.P., Stihler, S.D., Power, J.A., Searcey, S., 2010. Catalog of earthquake hypocenters at Alaskan Volcanoes: January 1 through December 2009. U.S. Geol. Sur. Data Series, 531 http://pubs.usgs.gov/ds/531.

Druitt, T.H., Young, S.R., Baptie, B., Bonadonna, C., Calder, E.S., Clarke, A.B., Cole, P.D., Harford, C.L., Herd, R.A., Luckett, R., Ryan, G., Voight, B., 2002. Episodes of cyclic Vulcanian explosive activity with fountain collapse at Soufrière Hills Volcano, Montserrat. In: Druitt, T.H., Kokleaar, B.P. (Eds.), The eruption of Soufriére Hills volcano, Montserrat, from 1995 to 1999: Geological Society of London, Memoirs, 21, pp. 281–306.

Ekstrand, A.L., Webley, P.W., Garay, M.J., Dehn, J., Prakash, A., Nelson, D.L., Dean, K.J., Steensen, T., 2013. A multi-sensor plume height analysis of the 2009 Redoubt eruption. J. Volcanol. Geotherm. Res. 259, 170–184.

Fee, D., McNutt, S.R., Lopez, T.M., Arnoult, K.M., Szuberla, C.A.L, Olson, J.V., 2013. Combining Local and Remote Infrasound Recordings from the 2009 Redoubt Volcano Eruption. J. Volcanol. Geotherm. Res. 259, 100–114.

Fehler, M., 1983. Observations of volcanic tremor at Mount St. Helens volcano. Journal of Geophysical Research 88, 3476–3484.

Foulger, G.R., Julian, B.R., Hill, D.P., Pitt, A.M., Malin, P.E., Shalev, E., 2004. Non-double-couple microearthquakes at Long Valley caldera, California, provide evidence for hydraulic fracturing. Journal of Volcanology and Geothermal Research 132, 45–71.

Fujita, E., Ukawa, M., Yamamoto, E., Okada, Y., Kikuchi, M., 2009. Volcanic Earthquakes and Tremors Associated with the 2000 Miyakejima Volcano Eruption. Journal of Geography 110, 191–203 in Japanese, with English Abstr.

Garces, M.A., McNutt, S.R., 1997. Theory of the airborne sound field generated in a resonant magma conduit. Journal of Volcanology and Geothermal Research 78, 155–178.

Green, D.N., Neuberg, J., 2006. Waveform classification of volcanic low-frequency earthquake swarms and its implication at Soufrière Hills Volcano, Montserrat. Journal of Volcanology and Geothermal Research 153, 51–63.

Hagerty, M.T., Schwartz, S.Y., Garcés, M.A., Protti, M., 2000. Analysis of seismic and acoustic observations at Arenal Volcano, Costa Rica, 1995–1997. Journal of Volcanology and Geothermal Research 101, 27–65.

Hammer, C., Neuberg, J.W., 2009. On the dynamical behaviour of low-frequency earthquake swarms prior to a dome collapse of Soufrière Hill volcano, Montserrat. Geophysical Research Letters 36.

Haney, M.M., van Wijk, K., Preston, L.A., Aldridge, D.F., 2009. Observation and modeling of source effects in coda wave interferometry at Pavlof volcano. The Leading Edge 28, 554–560.

Hardebeck, J.L., Shearer, P.M., 2002. A new method for determining first-motion focal mechanisms. Bulletin of the Seismological Society of America 92, 2264–2276.

Harrington, R.M., Brodsky, E.E., 2007. Volcanic hybrid earthquakes that are brittle-failure events. Geophysical Research Letters 34.

Hellweg, M., 2000. Physical models for the source of Lascar's harmonic tremor. Journal of Volcanology and Geothermal Research 101, 183–198.

Iverson, R.M., Dzurisin, D., Gardner, C.A., Gerlach, T.M., LaHusen, R.G., Lisowski, M., Major, J.J., Malone, S.D., Messerich, J.A., Moran, S.C., Pallister, J.S., Qamar, A.I., Schilling, S.P., Vallance, J.W., 2006. Dynamics of seismogenic volcanic extrusion at Mount St Helens in 2004–05. Nature 444, 439–443.

Jellinek, A.M., Bercovici, D., 2011. Seismic tremors and magma wagging during explosive volcanism. Nature 470, 522–525.

Johnson, J.B., Lees, J.M., 2000. Plugs and chugs–seismic and acoustic observations of degassing explosions at Karymsky, Russia and Sangay, Ecuador. Journal of Volcanology and Geothermal Research 101, 67–82.

Jousset, P., Neuberg, J., Sturton, S., 2003. Modelling the time-dependent frequency content of low-frequency volcanic earthquakes. Journal of Volcanology and Geothermal Research 128, 201–223.

Julian, B.R., 1994. Volcanic tremor: nonlinear excitation by fluid flow. Journal of Geophysical Research 99, 11859–11877.

Lahr, J.C., Chouet, B.A., Stephens, C.D., Power, J.A., Page, R.A., 1994. Earthquake classification, location, and error analysis in a volcanic environment: implications for the magmatic system of the 1989–1990 eruptions at Redoubt Volcano, Alaska. Journal of Volcanology and Geothermal Research 62, 137–152.

Lees, J.M., Ruiz, M., 2008. Non-linear explosion tremor at Sangay, Volcano, Ecuador. Journal of Volcanology and Geothermal Research 176, 170–178.

Lees, J.M., Gordeev, E.I., Ripepe, M., 2004. Explosions and periodic tremor at Karymsky volcano, Kamchatka, Russia. Geophysical Journal International 158, 1151–1167.

Lees, J.M., Johnson, J.B., Ruiz, M., Troncoso, L., Welsh, M., 2008. Reventador Volcano 2005: Eruptive activity inferred from seismo-acoustic observation. Journal of Volcanology and Geothermal Research 176, 179–190.

Lesage, P., Mora, M.M., Alvarado, G.E., Pacheco, J., Métaxian, J., 2006. Complex behavior and source model of the tremor at Arenal volcano, Costa Rica. Journal of Volcanology and Geothermal Research 157, 49–59.

MacAyeal, D.R., Okal, E.A., Aster, R.C., Bassis, J.N., 2008. Seismic and hydroacoustic tremor generated by colliding icebergs. Journal of Geophysical Research 113.

Malone, S., Haulter, A., 2003. How glacier-quakes can mimic low-frequency volcanic earthquake seismograms. EGS-AGU-EUG Joint Assembly, VGP14-ITU2P-0255.

Malone, S.D., Qamar, A., 1984. Repetitive micro-earthquakes as a source for volcanic tremor at Mount St. Helens. EOS Transactions American Geophysical Union 65, 1001 Abstr.

Martin, S., Drucker, R., Aster, R., Davey, F., Okal, E., Scambos, T., Macayeal, D., 2010. Kinematic and seismic analysis of giant tabular iceberg breakup at Cape Adare, Antarctica. Journal of Geophysical Research 115.

Maryanto, S., Iguchi, M., Tameguri, T., 2008. Constraints on the source mechanism of harmonic tremors based on seismological, ground deformation, and visual observations at Sakurajima volcano, Japan. Journal of Volcanology and Geothermal Research 170, 198–217.

Matoza, R.S., Garcés, M.A., Chouet, B.A., D'Auria, L., Hedlin, M.A.H., De Groot Hedlin, C., Waite, G.P., 2009. The source of infrasound associated with long-period events at Mount St. Helens. Journal of Geophysical Research 114, B04305.

Moran, S.C., Malone, S.D., Qamar, A.I., Thelen, W.A., Wright, A.K., Caplan-Auerbach, J., 2009. Seismicity Associated with Renewed Dome Building at Mount St. Helens, 2004–2005. In: Sherrod, D.R., Scott, W.E., Stauffer, P.H. (Eds.), A Volcano Rekindled: The Renewed Eruption of Mount St. Helens, 2004–2006: U.S. Geological Survey Professional Paper 1750, pp. 27–60.

Neuberg, J., 2000. Characteristics and causes of shallow seismicity in andesite volcanoes. Philosophical Transactions of the Royal Society of London A 358, 1533–1546.

Neuberg, J., Baptie, B., Luckett, R., Stewart, R., 1998. Results from the broadband seismic network on Montserrat. Geophysical Research Letters 25, 3661–3664.

Neuberg, J.W., Tuffen, H., Collier, L., Green, D., Powell, T., Dingwell, D., 2006. The trigger mechanism of low-frequency earthquakes on Montserrat. Journal of Volcanology and Geothermal Research 153, 37–50.

Ozerov, A., Ispolatov, I., Lees, J., 2003. Modeling Strombolian eruptions of Karymsky volcano, Kamchatka, Russia. Journal of Volcanology and Geothermal Research 122, 265–280.

Powell, T.W., Neuberg, J., 2003. Time dependent features in tremor spectra. Journal of Volcanology and Geothermal Research 128, 177–185.

Power, J.A., Lalla, D.J., 2010. Seismic Observations of Augustine Volcano, 1970–2007. In: Power, J.A., Coombs, M.L., Freymueller, J.T. (Eds.), The 2006 Eruption of Augustine Volcano, Alaska: U.S. Geological Survey Professional Paper 1769, pp. 1–38.

Power, J.A., Lahr, J.C., Page, R.A., Chouet, B.A., Stephens, C.D., Harlow, D.H., Murray, T.L., Davies, J.N., 1994. Seismic evolution of the 1989–1990 eruption sequence of Redoubt Volcano, Alaska. Journal of Volcanology and Geothermal Research 62, 69–94.

Power, J.A., Stihler, S.D., Chouet, B.A., Haney, M.M., Ketner, D.M., 2013. Seismic observations of Redoubt Volcano, Alaska—1989–2010 and a conceptual model of the Redoubt Magmatic System. J. Volcanol. Geotherm. Res. 259, 31–44.

Prejean, S.G., Ellsworth, W.L., 2001. Observations of earthquake source parameters at 2 km depth in the Long Valley caldera, eastern California. Bulletin of the Seismological Society of America 91, 165–177.

Reasenberg, P.A., Oppenheimer, D., 1985. FPFIT, FPPLOT, and FPPAGE: Fortran computer programs for calculating and displaying earthquake fault-plane solutions. U.S. Geological Survey Open-File Report 85–739. .

Ripepe, M., Delle Donne, D., Lacanna, G., Marchetti, E., Ulivieri, G., 2009. The onset of the 2007 Stromboli effusive eruption recorded by an integrated geophysical network. Journal of Volcanology and Geothermal Research 182, 131–136.

Rowe, C.A., Aster, R.C., Kyle, P.R., Dibble, R.R., Schlue, J.W., 2000. Seismic and acoustic observations at Mount Erebus Volcano, Ross Island, Antarctica, 1994–1998. Journal of Volcanology and Geothermal Research 101, 105–128.

Ruiz, M.C., Lees, J.M., Johnson, J.B., 2006. Source constraints of Tungurahua volcano explosion events. Bulletin of Volcanology 68, 480–490.

Schaefer, J.R.G., ed., 2012. The 2009 Eruption of Redoubt Volcano, Alaska: Alaska Division of Geological & Geophysical Surveys Report of Investigations 2011–5, 45p.

Schlindwein, V., Wassermann, J., Scherbaum, F., 1995. Spectral analysis of harmonic tremor signals at Mt. Semeru volcano, Indonesia. Geophysical Research Letters 22.

Stephens, C.D., Chouet, B.A., 2001. Evolution of the December 14, 1989 precursory long-period event swarm at Redoubt Volcano, Alaska. Journal of Volcanology and Geothermal Research 109, 133–148.

Thelen, W., West, M., Senyukov, S., 2010. Seismic characterization of the fall 2007 eruptive sequence at Bezymianny Volcano, Russia. Journal of Volcanology and Geothermal Research 194, 201–213.

Tuffen, H., Smith, R., Sammonds, P.R., 2008. Evidence for seismogenic fracture of silicic magma. Nature 453, 511–514.

Umakoshi, K., Takamura, N., Shinzato, N., Uchida, K., Matsuwo, N., Shimizu, H., 2008. Seismicity associated with the 1991–1995 dome growth at Unzen Volcano, Japan. Journal of Volcanology and Geothermal Research 175, 91–99.

Voight, B., 1988. A method for prediction of volcanic eruptions. Nature 332, 125–130.

Wallace, K.L., Schaefer, J.R., Coombs, M.L., 2013. Character, mass, distribution, and origin of tephra-fall deposits from the 2009 eruption of Redoubt Volcano. Alaska. J. Volcanol. Geotherm. Res. 259, 145–169.

Wessale, M.S., Pesicek, J.D., Syracuse, E.M., Thurber, C.H., DeShon, H.R., Power, J.A., Prejean, S.G., 2010. Comparison of Seismicity Preceding the 1989–1990 and 2009 Eruptions of Redoubt Volcano, Alaska. Abstract S21B-2037 presented at 2010 Fall Meeting, AGU, San Francisco, Calif., 13–17 Dec.